China Ocean Eng., 2019, Vol. 33, No. 1, P. 103–113
DOI: 10.1007/s13344-019-0011-y, ISSN 0890-5487
http://www.chinaoceanengin.cn/ E-mail: coe@nhri.cn

Experimental Study of Wave Attenuation in Trapezoidal Floating Breakwaters

A.H. Nikpour[a], M.N. Moghim[a, *], M.A. Badri[b]

[a]Department of Civil Engineering, Isfahan University of Technology, Isfahan P.O. Box 84156, Iran

[b]Research Institute for Subsea Science and Technology, Isfahan University of Technology, Isfahan P.O. Box 84156, Iran

Received January 7, 2018; revised August 22, 2018; accepted September 28, 2018

Abstract

A comprehensive experimental study was carried out on the regular wave attenuation with a trapezoidal pontoon-type floating breakwater (FB) in deep water. The functionalities of two simple FB geometries consist of a rectangle and a trapezoid with the slope of 60° were investigated under the wave attack. A two-dimensional wave flume was used in the experiment; the incident, transmitted waves, mooring line forces and motion responses of the floating breakwaters were measured. Also the influence of the sea state conditions (incident wave height and wave period) and structural parameters (draught of the structure) were investigated using the trapezoidal FB. Our experimental results indicated that the trapezoidal FB significantly reduced the wave transmission and mooring line force when compared with rectangular FBs. A new formula was developed in order to predict the value of the transmission coefficient in trapezoidal FBs with the slope of 60°. Experimental data showed to be consistent with the results of the formula.

Key words: regular waves, floating breakwater (FB), wave flume, trapezoid, mooring line force, transmission

Citation: Nikpour, A. H., Moghim, M. N., Badri, M. A., 2019. Experimental study of wave attenuation in trapezoidal floating breakwaters. China Ocean Eng., 33(1): 103–113, doi: 10.1007/s13344-019-0011-y

1 Introduction

Breakwaters are the most important elements in coastal construction protecting the coasts against wind wave energy. They are divided into fix floating categories. Recently, FBs, berth and floating bridge have caught increasing interests because of lower investment and being environmental friendly. In particular, FBs are preferable over rubble-mound breakwaters in reducing costs and wave agitation under specific conditions such as short wave period, small wave heights and large water depth. FBs can automatically accommodate for depth changes, and can be used at sites with large water depth or poor foundation conditions. In recent years, because of the above-mentioned advantages of using FBs, many types of FBs such as pontoon, catamaran, circular pipe and scarp tire breakwaters have been designed and constructed (Hales, 1981).

In the floating structures, the incident wave is partially reflected, transmitted and dissipated. Energy dissipation is normally due to damping, friction and generation of eddies at the edges of a breakwaters.

In order to enhance the performance of FBs, various solutions have been investigated. As an example, several studies have been performed to optimize the geometry of the FB as an important solution. As a result, several geometries have been proposed and experimentally tested to show a progressive improvement on the performance of FBs. The hydrodynamics of the rectangular cross-section FBs have been investigated numerically and experimentally. Efforts have been made to find the most effective geometry and configuration of rectangular FBs (Cheng et al., 2013).

The most common configuration of FB is a single pontoon with different geometries, e.g., Mani (1991), Drimer et al. (1992), Yao et al. (1993), Abul-Azm and Gesraha (2000), Koutandos et al. (2004), Koftis and Prinos (2005), Gesraha (2006), Elchahal et al. (2008), Peña et al. (2011), He et al. (2012), Abdolali et al. (2012), Koraima and Rageh (2013) and Moghim and Botshekan (2017). In order to increase the inertia without changing the total mass, two single pontoons are connected to construct a double pontoons FB. Double pontoons FB may attenuate waves in the same way as a single pontoon, but in addition double pontoons FB reduces the wave field through turbulence between the two floating bodies, e.g., William and Abu-Azm (1997), Murali and Mani (1997), Tang et al. (2011) and Ji et al. (2015).

Mani (1991) has studied a Y-frame FB with a row of cylinders installed under a pontoon breakwater in regular waves. This structure disturbs water particle orbit to reduce

*Corresponding author. E-mail: moghim@cc.iut.ac.ir

wave. For most of the FBs, if B/L ratio (B is the width of the breakwater and L, the wave length) is in the range of 0.45–1.70, the transmission coefficient (C_t) could be below 0.5.

Murali and Mani (1997) have developed an improved cage FB system in regular waves (Fig. 1). The basic cost-effective Y-frame FB configuration (Mani, 1991) has been adopted for their system. The breakwater comprises two trapezoidal pontoons of the width B spaced at a clear distance b and fixed with two rows of equally spaced piles with a certain gap to the pile diameter ratio (G/D). Murali and Mani have shown that by using the optimal combination of effective parameters (with G/D=0.22, dr/d=0.46, b/B=1.0, and a maximum initial tension corresponding to 22.5% of the total displacement of the pontoons), for a large value of $H_i/(gT^2) > 0.010$, the system could effectively restrict C_t to be under 0.1. This performance is comparable with conventional breakwaters such as rubble mound breakwaters. Murali and Mani have shown that with a desired mooring line pretension, the change of the mooring line stiffness from 5 to 50 N/mm does not modify the performance of the FB, but the use of mooring lines with adequate stiffness is essential.

The hydrodynamic properties of a dual pontoon FB consisting of a pair of rectangular section floating cylinders that are connected by a rigid deck have been investigated theoretically by William and Abu-Azm (1997). It has been shown that the structural draught, the space between the pontoons and the mooring line stiffness strongly have an influence on the wave reflection. Also, Weng and Chou (2007) investigated the hydrodynamic properties of a dual pontoon FB consisting of a pair of rectangular sectional floating cylinders connected by a rigid framework.

Koftis and Prinos (2005) have numerically studied a new shape of a pontoon-type FB with improved hydrodynamic characteristics in monochromatic waves to understand the mechanism of wave energy dissipation in the trapezoidal and rectangular cross section FBs. They showed an overall improvement in the functionality of trapezoidal FB in comparison with the typical rectangular FB due to the geometry of the structure. The trapezoidal FB reduces the wave transmission and increases energy dissipation in its inclined front face. Moreover, their study showed a greater

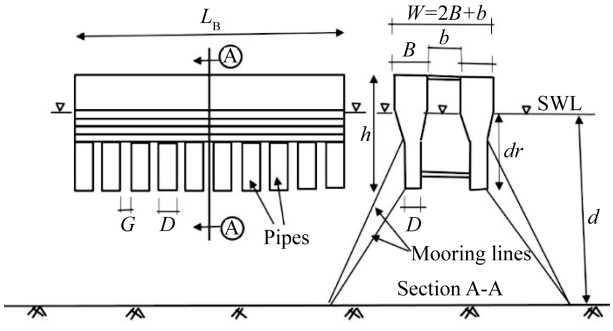

Fig. 1. Schematic view of the cage FB system (Murali and Mani, 1997).

vortex flow near the sharp edges, vaster area with vortex and also dissipating part of wave energy due to the flow run up on inclined face in the trapezoidal FB compared with the rectangular FB.

Gesraha (2006) investigated π shaped FB and compared its performance with the rectangular one with the same mass and under-tip clearance in an incident train of monochromatic wave. It was found that adding side-boards experiences lower exciting forces and heave damping coefficient, but other hydrodynamic coefficients are higher for the present configuration. The resulting wave transmission is lower within the range of incident wave frequency tested.

Peña et al. (2011) conducted experiments on different π-type models by taking π-type model of Baiona port as the base. Three new designs with various dimensions have been tested and the following observations have been concluded:

(1) The width of FB is a fundamental design parameter to achieve greater wave dissipation.

(2) FBs malfunction for long wave conditions.

(3) Minimal improvements have been achieved by increasing lateral fins.

(4) Neither rigid nor elastic mooring lines have significant effect on C_t.

Abdolali et al. (2012) investigated, both numerically and experimentally, the effect of width and draught of the body of π type FBs subject to regular waves constrained to move only vertically. Their studies showed that the attached plate can improve the efficiency of breakwater by increasing the energy dissipation around edges and reflection in seaside.

Ji et al. (2015) conducted a 2D experiment to study a new type of FB which has a mesh cage underneath under regular wave conditions. Increasing the inertia without changing the total mass was the basic purpose of the design. Three other types – including the same model without a mesh cage, a model with a mesh cage and rubber balls in it, and a simple rectangular box – were also constructed. It was observed that the greatest efficiency can be achieved by using the traditional cylindrical model with a mesh cage and balls.

Although many researchers tried to improve the efficiency of the FBs, the research developments are still very limited and the gap between current technology and demands is large.

Based on Gesraha (2006) investigation, the most common FB in the industry is the π shaped FB which is a rectangular caisson with two vertical plates protruding downward from the sides. A vertical plate significantly enhanced the efficiency of the structure, increasing dissipation and therefore reducing transmission but it can enhance wave reflection. In this study, the effect of the trapezoidal FB with simple geometry on regular wave attenuation has been tested by performing comprehensive experiments. The functionality of the rectangular and trapezoidal FBs were tested and compared. The influence of incident wave characterist-

ics (wave height and wave period) and also structural parameter (draught of the structure) has been investigated on FB's performance, mooring line forces and structure motions for two different FB geometries (i.e., rectangular and trapezoidal FBs).

2 Laboratory experiments and facilities

2.1 Model design

The experiment was carried out in a 110-m-long, 3-m-wide, and 2.50-m-deep towing tank located in the Research Institute for Subsea Science and Technology at Isfahan University of Technology (IUT), Isfahan, Iran (Fig. 2). The sidewalls of the wave tank are made of concrete, with three underwater observation windows. The tank is equipped with a mechanical–electrical plunger-type wave maker that placed at the beginning of the flume. It generates regular waves with a wide range of wave periods and wave heights. Upward and downward plunger movement is controlled by a potentiometer control box. The FB test model is located approximately 40 m away from the wave generator.

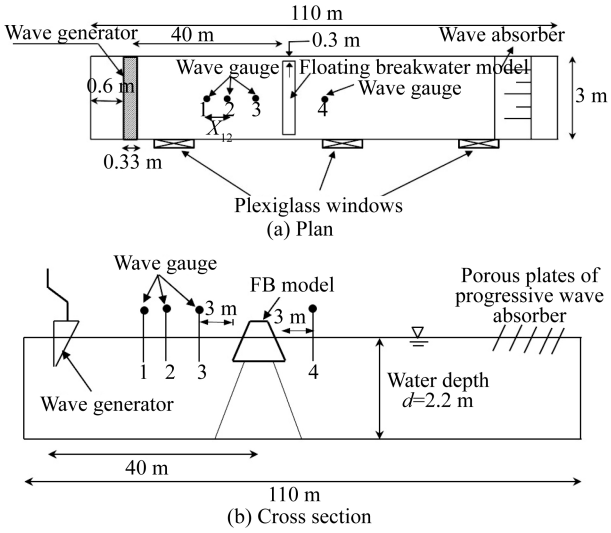

Fig. 2. Schematic view of the experimental setup.

A progressive wave absorber consisting of five porous plates with different porosities, decreasing in the direction of incident wave, is placed at the downstream end of the wave tank to minimize the reflection effects of transmitted waves (Fig. 3).

Four capacitive wave gauges are installed in the flume to record water level fluctuations. The sampling frequency during the experiments is 50 Hz. Three capacitive wave gauges are installed in the seaside part of the flume, between the wave generator and structure model at constant water depth for separating the reflected wave height (H_r) from incident wave height (H_i) by the Mansard and Funke method. To calculate the relative distance between the wave gauges, the suggestion proposed by Mansard and Funke (1980) has been followed as follows:

Fig. 3. Wave absorber of IUT.

$$X_{12} = L/10,\ \ L/6 \leqslant X_{13} \leqslant L/3,$$
$$X_{13} \neq L/5,\ \ X_{13} \neq 3L/10, \tag{1}$$

where L is the wave length, X_{12} is the distance between the first two wave gauges in the line of wave propagation, X_{13} is the distance between the first and third wave gauges in the line of wave propagation.

According to Abdolali and Kolahdoozan (2011), if the wave gauge is close to the model test and the water depth is constant, the location of the wave gauge has no significant effect on the reflection coefficient. Therefore, the first wave gauge was installed 3 m from the test model as shown in Fig. 2. One wave gauge was placed in leeward of the test model to measure the transmitted wave height (H_t). Maximum run time for each experimental test was about 35 s, so wave reflections from the wave absorber could not influence the transmitted wave height during this run time.

The FB model was moored to the flume bed by four taut mooring lines. Based on Murali and Mani (1997), the mooring lines stiffness from 5 to 50 N/mm has no effect on the performance of the FB. In the present study, the stiffness of mooring lines was about 25 N/mm. One dimensional S-type load cell with the capacity of 50 kgf was used to record the seaward mooring line forces (Fig. 4). Also it was used to set the initial tension force of mooring line forces before each experimental test. The S-type load cell was fabricated using stainless steel material with the height of 61 mm and thickness of 11.7 mm, being made waterproof. The load cell was calibrated and found to be linear up to 350 N, and the calib-

Fig. 4. Load cell and equipment being used to measure the mooring line forces.

ration constant was 0.021 $Nm^{-1}V^{-1}$. The load cell was generally calibrated before and after each test by applying a series of loads to the cantilever using a mechanical load – tightener. The sampling frequency during the experiments is 50 Hz to ensure that no sharp peak in data is lost.

In order to record the FB motion, two mechanical-electrical draw wire sensors were used to record the horizontal and vertical motions of FB (Fig. 5). The FB's centers of gravity motions were recorded by using these sensors. The sampling frequency during the experiments was 50 Hz.

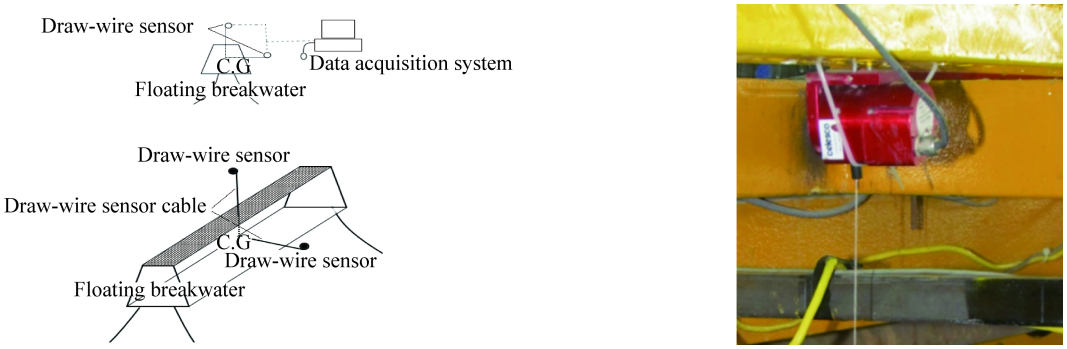

Fig. 5. Mechanical-electrical draw wire sensor being used to measure the structure motion.

2.2 Ranges of sea state and structural parameters

The geometries of pontoon FB models are rectangular and trapezoidal with the slope of 60° (Fig. 6). The structures are made of water-resistant wood. In order to reach the required draughts, small concrete pieces are used inside the models. Pieces made of extruded polystyrene foam are used around the concrete weights to prevent the movement of pieces and keep structure's balance. The length of the structure (L_B) is 2.4 m, the width (B) 0.43 m and the height (h) 0.34 m. The draught of the structure (dr) ranges from 0.12 to 0.24 m.

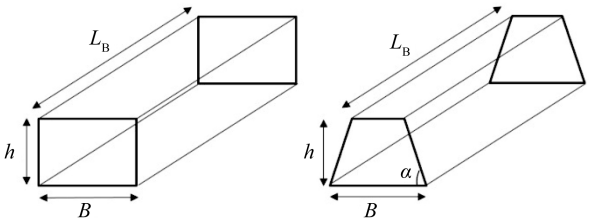

Fig. 6. Rectangular and trapezoidal breakwaters as test models.

Four 2-mm galvanized steel cables were employed in order to moor the structures. Sannasiraj et al. (1998) analyzed the effect of mooring lines arrangement on floating structures in three states. Their study revealed that mooring lines arrangement may not significantly affect the wave transmission coefficient but it can affect the mooring line force. Fig. 7 shows the mooring configuration that was used in the present study. The mooring cables were connected to the bottom of the flume at a slope ratio of 3:1. According to Peña et al. (2011), initial tension in mooring line cables does not significantly affect the transmission coefficient but it creates reduction in the movement of floating structures. Therefore, the cables used in our experiments were pre-tensioned using turnbuckles.

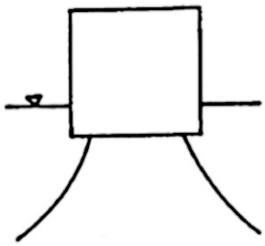

Fig. 7. Schematic view of mooring lines arrangement.

The dimensions of the sea state parameters consist of the incident wave height (H_i), wave period (T), water depth at the structure (d) and the wave length (L) are listed in Table 1. In accordance with the dimensions of laboratory facilities and the test wave conditions, the proposed scale is 1:20. In all experiments, the water depth is 2.2 m. The regular prototype wave periods range from 4.47 to 5.81 s, and the prototype wave heights range from 0.50 to 2.68 m. According to the experimental model scales, the experimental wave periods (T) range from 1.0 to 1.3 s, and the experimental wave heights (H_i) range from 0.025 to 0.134 m. All the experiments were performed with non-breaking regular waves under deep water condition ($d/L > 0.5$).

Table 1 Range of the dimensions of the sea state parameters

Parameter	Range
Wave period T (s)	1.0–1.3
Wave length L (m)	1.26–2.63
Wave height H_i (m)	0.025–0.134
Water depth d (m)	2.19

3 Data analysis

The effects of sea state and structural parameters on the efficiency of rectangular and trapezoidal FBs were investig-

ated by measuring the wave transmission and mooring line force. At the end of each part, the performance of rectangular and trapezoidal FB is compared.

3.1 Wave transmission

3.1.1 *Wave height effect*

Fig. 8 indicates the wave height effect on the transmission coefficient (C_t=H_t/H_i) for trapezoidal FB. It can be seen that because of the breakwater motion, if the wave height with the same wave period increases, the transmission coefficient will decrease. The wave height effect on the heave and sway motions of trapezoidal FB is shown in Figs. 9 and 10, respectively. According to Figs. 9 and 10, the heave and sway motions are increasing by enlarging the wave height for constant values of the wave period. Fig. 11 shows a schematic layout of the wave height effect on the structure motions and mooring line stretch. Increasing heave and sway motions of FB would cause stretching the mooring line. From Fig. 11, it can be inferred wave transmission reduction since stretching of FB mooring line leads to relatively rigid behavior of the structure against incident wave.

3.1.2 *Effect of wave period*

Fig. 12 shows the effect of the wave period on the transmission coefficient with different values of the wave height for trapezoidal FB. It is observed that the wave period has significant effect on the transmission coefficient of trapezoidal FB. The higher value for the wave period leads to more transmission. An increase of the wave period leads to increasing the wave length and it causes harmonic mo-

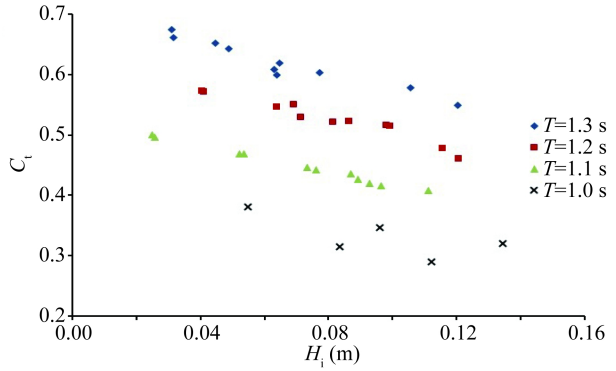

Fig. 8. Wave height effect on the transmission coefficient for trapezoidal FB (dr = 0.16 m and h = 0.34 m).

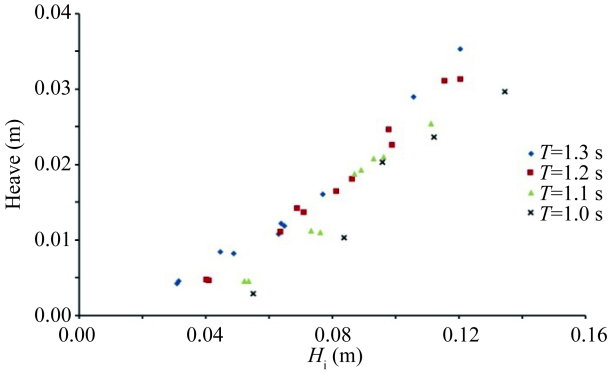

Fig. 9. Wave height effect on the heave motion for trapezoidal FB (dr = 0.16 m and h = 0.34 m).

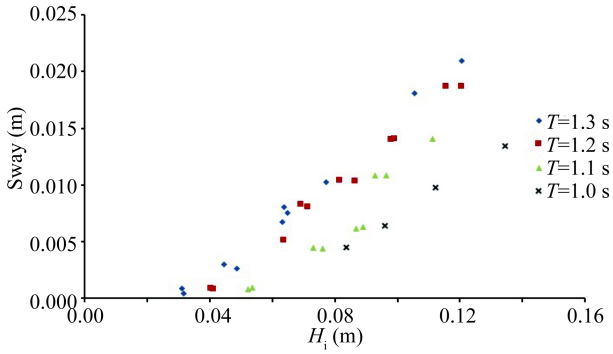

Fig. 10. Wave height effect on the sway motion for trapezoidal FB (dr = 0.16 m and h = 0.34 m).

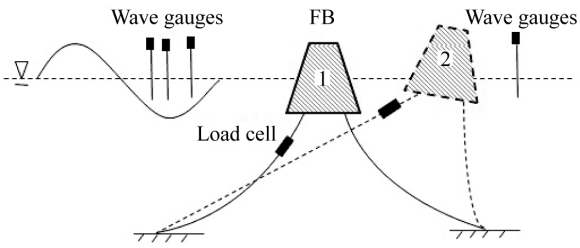

(a) Mooring line stretch and structural movement due to higher wave height

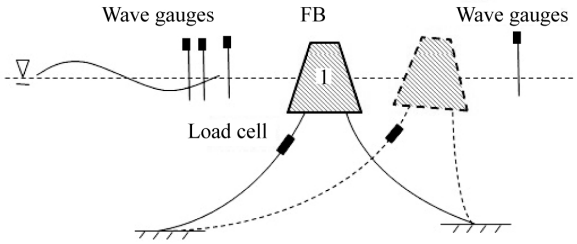

(b) Mooring line stretch and structural movement due to lower wave height

Fig. 11. Schematic layout of the wave height effect on the structure motion and mooring line stretch.

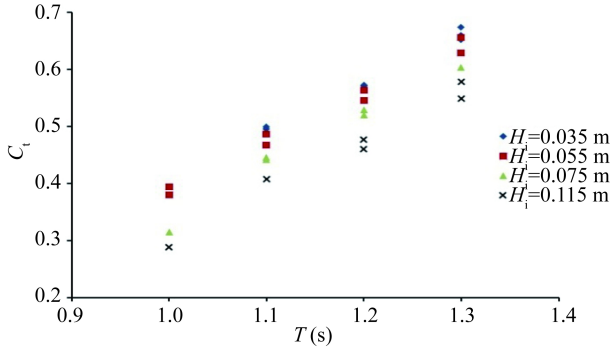

Fig. 12. Wave period effect on the transmission coefficient for trapezoidal FB (dr = 0.16 m and h = 0.34 m).

tion of FB and wave oscillation. It means that, by increasing the wave length, instead of confronting the structure against the wave, the structure is consistent with the wave oscillation and then the wave may pass easily through the structure.

The effects of the wave period on the heave and sway motions are shown in Figs. 13 and 14, respectively. According to Figs. 13 and 14, increasing the wave period for a constant value of wave height may enhance the heave and sway motions. It seems that further displacement of FB, represents the harmonic movement of the structure and wave oscillation and it leads to reducing the structure efficiency. Wave transmission could be effected by both the wave period and FB geometry. In other words, harmonic movement of the structure and wave oscillation could happen once the ratio of the FB width to wave length reduces and as a result the wave transmission would increase.

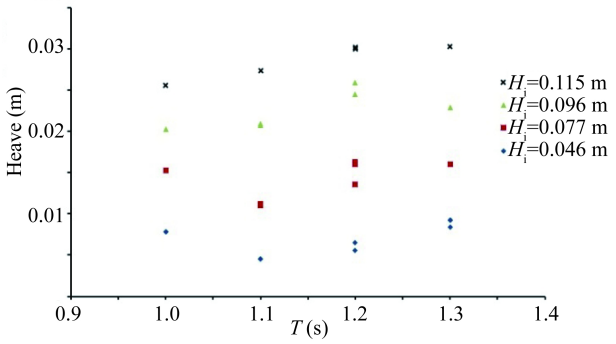

Fig. 13. Wave period effect on the heave motion for trapezoidal FB (dr = 0.16 m and h = 0.34 m).

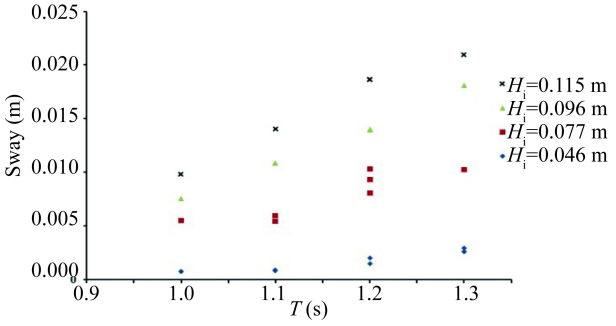

Fig. 14. Wave period effect on the sway motion for trapezoidal FB (dr = 0.16 m and h = 0.34 m).

3.1.3 *Draught effect*

The influence of the FB draught on the wave transmission coefficient for the same wave height and period for trapezoidal FB is shown in Fig. 15. Fig. 15 indicates that as the structural draught increases, the transmission coefficient would decrease. The reason for this reduction is that by increasing the draught of the structure, more part of its body is placed in the water and it can prevent transmitting the wave energy through the bottom of the structure. Also it seems

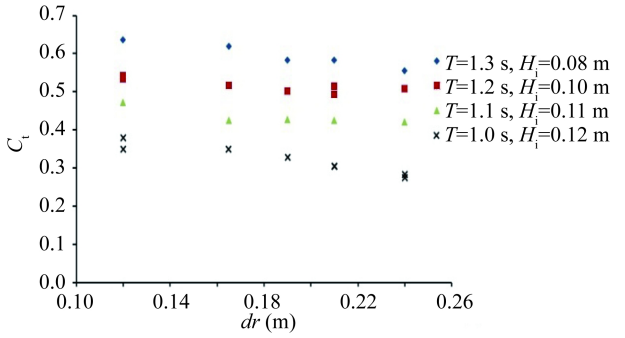

Fig. 15. Draught effect on the transmission coefficient for the same wave height and period for trapezoidal FB.

that by increasing the structural draught, the mass and inertia would be bigger and more wave energy dissipation can be expected.

3.1.4 *Dimensionless analysis*

The transmission coefficient in trapezoidal FBs depends on the following parameters which are introduced in Section 2.2:

$$C_t = f(H_i, T, \rho, g, \mu, B, dr). \tag{2}$$

Transmission coefficient can be expressed in the form of 4 non-dimensional parameters by the Buckingham Pi theorem. Non-dimensional parameters are reduced by using compounding method as shown below:

$$C_t = f'\left(\frac{gT^2}{B}, \frac{drH_i}{B^2}, \frac{\sqrt{gH_i}B}{\upsilon}\right). \tag{3}$$

The last dimensionless parameter in Eq. (3) is the Reynolds number ($Re = \sqrt{gH_i}B/\upsilon$) and the first dimensionless parameter is the Froude number ($F^2 = gT^2/B$). As the similarity requirements posed by the Froude and the Reynolds numbers can typically not be satisfied simultaneously, it is then necessary to decide the dominant force according to which the scaling must be done. In the present experimental research, the minimum value of the Reynolds number is about $Re_{min} \approx 2.1 \times 10^5$. The Froude number has to be maintained, but the Reynolds number will be strictly not required to use, so it may not be illuse, and it may not illogical to ignore the effect of viscosity and employ the Froude number. Therefore, Eq. (3) is simplified to the following:

$$C_t = f'\left(\frac{gT^2}{B}, \frac{drH_i}{B^2}\right). \tag{4}$$

Table 2 shows the range of non-dimensional parameters for the present experimental tests.

Fig. 16 indicates the variation of C_t versus drH_i/B^2 for the constant values of gT^2/B . It shows that for the constant value of gT^2/B, C_t will decrease by increasing drH_i/B^2. Fig. 17 shows the variation of C_t versus gT^2/B for the constant values of drH_i/B^2. It has be seen that for the constant value of drH_i/B^2, as gT^2/B gets bigger, C_t will increase. It can be concluded from Figs. 16 and 17 that in order to en-

Table 2 Range of non-dimensional parameters

Parameter	Range
drH_i/B^2	0.052–0.152
gT^2/B	22.8–38.5

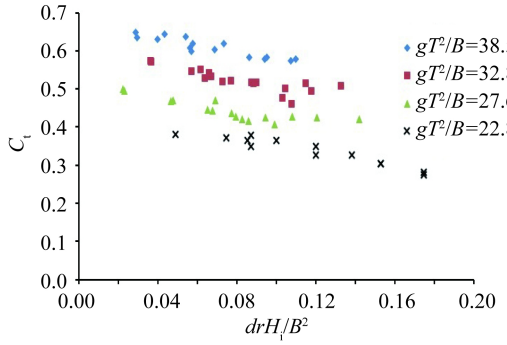

Fig. 16. Variation of C_t versus drH_i/B^2 with the constant values of gT^2/B for trapezoidal FB.

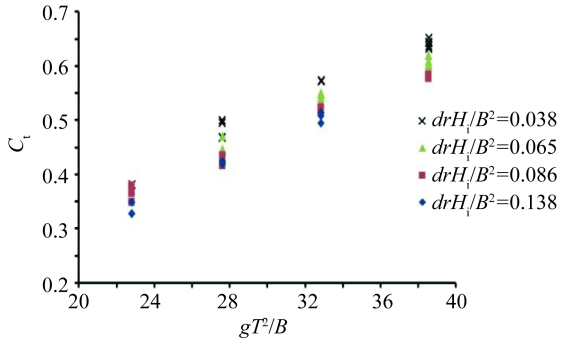

Fig. 17. Variation of C_t versus gT^2/B with the constant values of drH_i/B^2 for trapezoidal FB.

sure the shielded effect of the tested trapezoidal FBs (C_t < 0.5), drH_i/B^2 is larger than 0.1 or gT^2/B is smaller than 29.

By achieving the appropriate dimensionless parameter for describing the FB performance, a new formula for calculating the wave transmission coefficient of trapezoidal FB is proposed. To study the effect of drH_i/B^2 on the transmission coefficient for constant value of gT^2/B, different functions are evaluated and finally a power function is chosen as:

$$C_t = \alpha\left(\frac{drH_i}{B^2}\right)^{\beta}. \tag{5}$$

Regression analysis is used to find proper values of α and β for Eq. (5). Table 3 shows α and β for different values of gT^2/B. The effect of gT^2/B on the values of α and β is shown in Figs. 18 and 19. It can be seen that α depends on gT^2/B $\left(\alpha = \psi\left(\frac{gT^2}{B}\right)\right)$ and also β is almost constant for different values of gT^2/B. According to Table 3, the average value of β is around –0.11. Eq. (6) is used as a proper pattern to consider the effect of drH_i/B^2 on C_t.

Table 3 Values of α and β

gT^2/B	$>\alpha$	$>\beta$
38.55	0.47	−0.09
32.85	0.37	−0.13
27.60	0.33	−0.11
22.81	0.25	−0.13

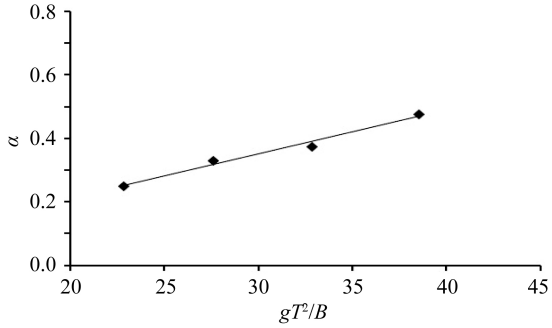

Fig. 18. Relation between gT^2/B and α.

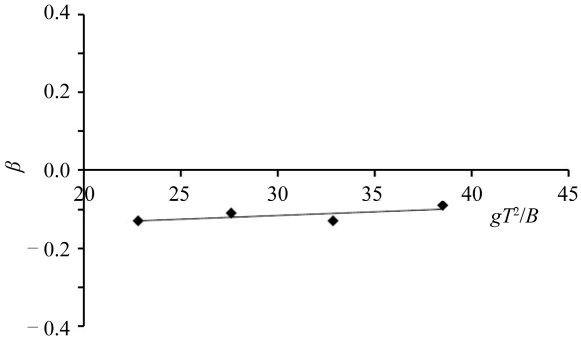

Fig. 19. Relation between gT^2/B and β.

$$C_t = \psi\left(\frac{gT^2}{B}\right)\left(\frac{drH_i}{B^2}\right)^{-0.11}. \tag{6}$$

In order to find a proper transmission coefficient formula, Eq. (6) can be rewritten as follows:

$$\psi\left(\frac{gT^2}{B}\right) = C_t \Big/ \left(\frac{drH_i}{B^2}\right)^{-0.11}. \tag{7}$$

The value of $\psi\left(\frac{gT^2}{B}\right)$ is evaluated by using Eq. (7)(Fig. 20). In order to find a proper function to estimate $\psi\left(\frac{gT^2}{B}\right)$, different algebraic functions such as linear and power functions are examined and finally Eq. (8) is derived in order to calculate the transmission coefficient in trapezoidal FBs with the slope of 60°.

$$C_t = 0.0111\left(\frac{drH_i}{B^2}\right)^{-0.11}\left(\frac{gT^2}{B}\right)^{1.02}. \tag{8}$$

3.1.5 *Verification of the derived formula*

The performance of the formula in predicting the wave transmission for trapezoidal FBs is evaluated using the

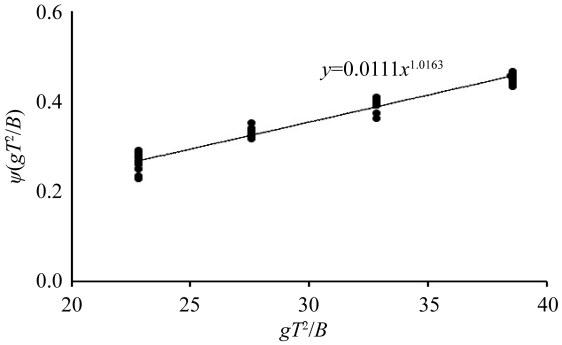

Fig. 20. Variation of $\psi\left(gT^2/B\right)$ with gT^2/B by using the present experimental data for trapezoidal FB.

present experimental data. The evaluation has been done by using normalized root mean square error (*NRMSE*), percentage of relative error (E) and the square of the correlation factor (R^2) for which a squared correlation factor close to 1 denotes full agreement. These are computed according to:

$$NRMSE = \sqrt{\frac{\sum (Y-X)^2}{\sum (Y-\bar{Y})^2}}; \tag{9}$$

$$E = \frac{100}{N}\sum_{i=1}^{N}\left|\frac{Y-X}{Y}\right|; \tag{10}$$

$$R^2 = \left\{\frac{N\sum XY - \left(\sum X\right)\left(\sum Y\right)}{\sqrt{\left[N\sum X^2 - \left(\sum X\right)^2\right]\left[N\sum Y^2 - \left(\sum Y\right)^2\right]}}\right\}^2, \tag{11}$$

where X is the calculated value using Eq. (8), Y is the observation data, $\bar{Y}$ is the average value for the observation data and N is the total number of realizations. Based on the validation indices, R^2 = 0.97, *NRMSE* = 0.18 and E= 3.1%. Fig. 21 compares the experimental and predicted C_t with good agreement.

3.1.6 *Wave transmission comparison of rectangular and trapezoidal FB*

Fig. 22 shows the effect of the FBs structure draught on the transmission coefficient by keeping the value of the wave period and height the same in trapezoidal and rectangular cross sections. According to Fig. 22, if the structural draught increases, the wave transmission would decrease for both cross sections. In addition, it can be concluded from Fig. 22 that for a constant value of the wave period and height, the wave transmission of trapezoidal cross section is less than that of rectangular one. This is due to the geometry of trapezoidal FB in which some part of the wave energy is dissipated due to wave run up on the inclined face of the structure. Interaction of the return flow that run-down the structure slope with the next run-up flow on the structure slope would dissipate more energy.

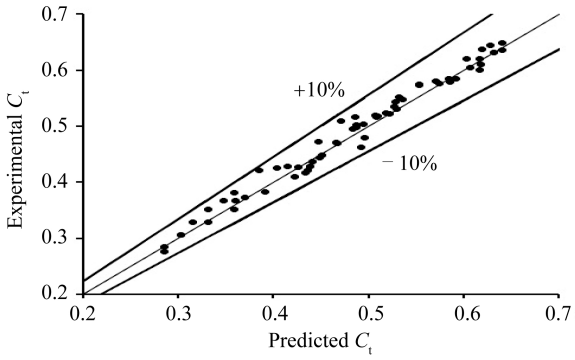

Fig. 21. Variation of the experimental C_t versus the predicted C_t using Eq. (8) for trapezoidal FB.

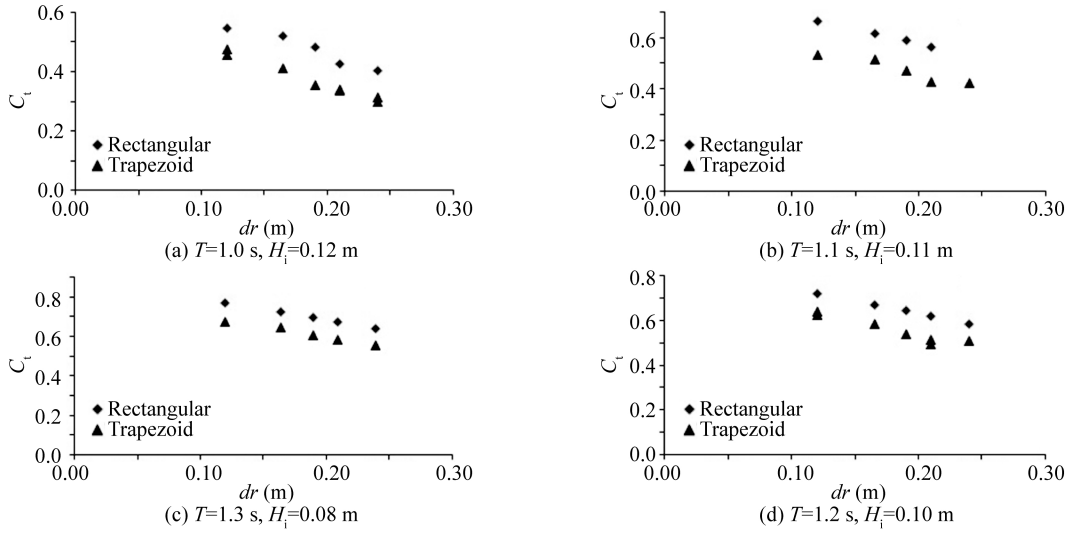

Fig. 22. Draught effect on the transmission coefficient for rectangular and trapezoidal cross sections.

3.2 Mooring line force

3.2.1 *Effect of the wave height on the mooring line force*

The effect of the wave height on the mooring line force while the wave period kept constant is shown in Fig. 23 for trapezoidal FB. According to Fig. 23 if the wave height gets larger, the mooring line force would increase linearly. As the wave energy is proportional to the square power of the wave height (H_i^2), by increasing the wave height, the wave energy and mooring line force would increase. In fact, increasing the wave height leads to bigger FB motion and as a result the semi rigid behavior of the structure could happen. Therefore, the structure can dissipate more wave energy, the efficiency of FB can be improved and the mooring line force would increase.

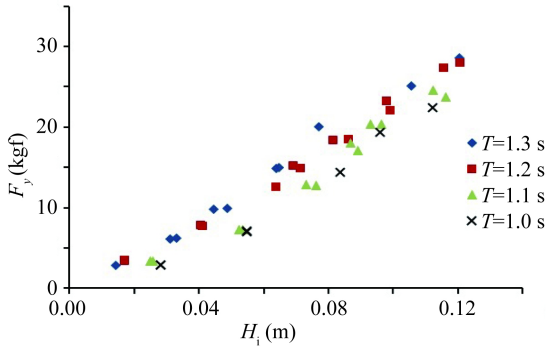

Fig. 23. Effect of the wave height on the mooring line force (dr=0.165 m) for trapezoidal FB.

3.2.2 *Effect of the wave period on the mooring line force*

The effect of wave period on mooring line force while the wave height kept constant is shown in Fig. 24 for trapezoidal FB. If the wave period increases, the mooring line force will increase as well.

3.2.3 *Effect of the draught on the mooring line force*

The influence of the FB draught on the mooring line force for the same wave height and period is shown in Fig. 25 for trapezoidal FB. It is observed that by increasing the

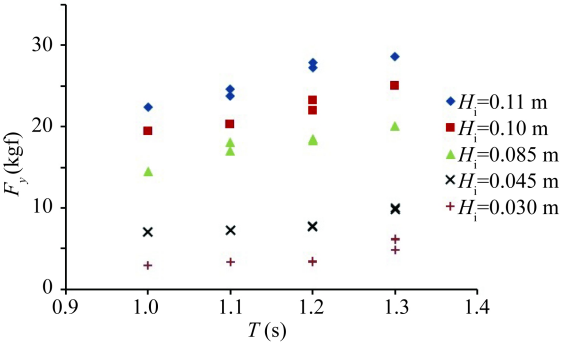

Fig. 24. Wave period on the mooring line force (dr=0.165 m) for trapezoidal FB.

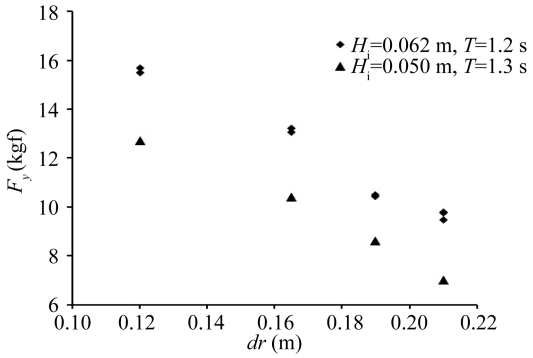

Fig. 25. Draught effect on the mooring line force for trapezoidal FB.

structural draught, the mooring line force will decrease in trapezoidal FB. The laboratory observation indicates that by increasing the structural draught, the run-up level will increase on the inclined face of trapezoidal FBs. Therefore, the vertical force due to water pressure will be higher on submerged inclined face of trapezoidal FBs which leads to decrease the mooring line forces.

3.2.4 *Mooring line force comparison of rectangular and trapezoidal FB*

The effect of the structural draught on the mooring line force while the wave height and period kept constant is shown in Fig. 26 for both trapezoidal and rectangular FBs. This figure shows that if the structural draught increases, the mooring line force will increase for rectangular FB because of larger mass and inertia of the structure. This structural behavior for the mooring line force versus the structural draught in rectangular FB is unlike the trapezoidal FB behavior. By the same values of the draught, wave height and wave period, the mooring line force in trapezoidal FB is smaller than that in rectangular FB for the following reasons:

(1) In trapezoidal FB, due to the vertical pressure force on the submerged inclined face during wave run up, the mooring line forces reduce unlike rectangular FB (Fig. 27).

(2) In trapezoidal FB, the wave force (F_W) is applied perpendicular to the inclined surface. This force decom-

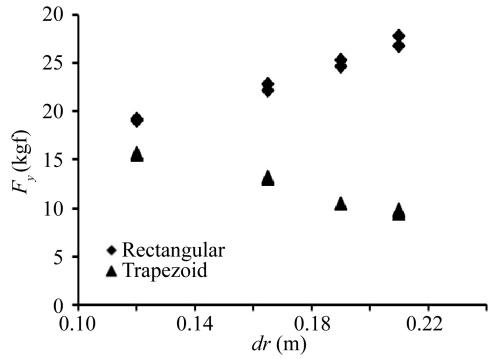

Fig. 26. Draught effect on the mooring line force for rectangular and trapezoidal FB (H_i=0.062 m and T=1.2 s).

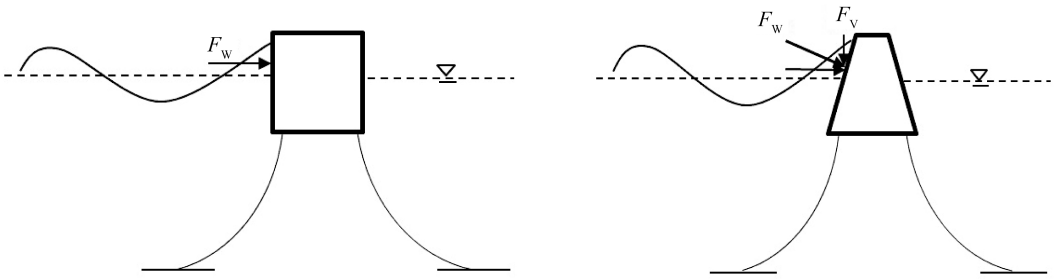

Fig. 27. Schematic view of applied wave force on rectangular and trapezoidal FB.

poses to the vertical and horizontal components. The vertical component of the wave force (F_V) can cause reduction in the mooring line force for trapezoidal FB (Fig. 27). But in rectangular FB the wave force is applied perpendicular to the vertical structure surface, so this force has no vertical component and cannot reduce the mooring line force.

4 Conclusions

In this paper, the performance of the proposed trapezoidal pontoon type FB was compared with the rectangular pontoon type FB by using experimental study at the towing tank located in the Research Institute for Subsea Science and Technology at IUT. A series of regular wave experiments were carried out to validate the new model. Also, the effect of sea wave parameters and geometric characteristics was investigated on the performance, mooring line force and structural motion. The following highlights were concluded from this study.

(1) If the structural draught, wave height and period are the same, less mooring line force and wave transmission could be observed in trapezoidal FB in comparison with that of rectangular FB. The reason could be related to the structural geometry because of the wave energy dissipation due to wave run up on the inclined face of trapezoidal structure, greater vortex flow near the sharp edges of the structure and also vaster area with vortex in trapezoidal FB. In addition, some wave energy dissipation occurs due to the interaction between the return flow that was the run down and the next run up flow on the structure slope.

(2) An increase in the wave height may lead to the increase of the heave, sway motion and mooring line force in trapezoidal FBs. Larger heave and sway motion of FB due to bigger wave height would cause the stretch in mooring line. Stretching of FB mooring line may lead to relatively rigid behavior of the structure against the incident wave, so the wave transmission could be reduced.

(3) The wave period was significantly affecting the FB response. A longer wave period will increase the wave length. By increasing the wave length, the structure will be consistent with the wave oscillation and the wave may pass easily through the structure.

(4) The major area of the structure will be covered in the water by increasing the draught. It could prevent the transmission of the wave energy through the bottom of the structure. Also, more mass and inertia due to larger structural draught could dissipate more wave energy, and therefore the transmission coefficient could be reduced.

(5) Increase in the structural draught will cause reduction and enlargement in the mooring line force for trapezoidal and rectangular FBs, respectively.

(6) A new formula ((Eq. (8)) with the selected non-dimensional parameter was derived to calculate the transmission coefficient in trapezoidal FBs with the slope of 60°. The performance of the formula was evaluated using the present experimental data and good agreement between the predicted and experimental data has been observed.

Acknowledgements

The authors wish to express their sincere thanks to the Research Institute for Subsea Science and Technology, Isfahan University of Technology (IUT) in Iran for providing experimental facilities.

References

Abdolali, A. and Kolahdoozan, M., 2011. Comparison of analytical methods of wave decomposition for evaluating reflection coefficient, *Journal of Marine Engineering*, 7(14), 105–116.

Abdolali, A., Franco, L., Bellotti, G. and Kolahdoozan, M., 2012. Hydraulic and numerical modeling of the performance of π-type floating breakwaters, *Proceeding of the 10th International Conference on Coasts, Ports and Marine Structures* (*ICOPMAS*), Tehran, Iran.

Abul-Azm, A.G. and Gesraha, M.R., 2000. Approximation to the hydrodynamics of floating pontoons under oblique waves, *Ocean Engineering*, 27(4), 365–384.

Cheng, L.H., Fen, C.Y., Li, Y.H. and Jiang, W.Y., 2013. Experimental study on a new type floating breakwater, *Proceedings of the 7th International Conference on Asian and Pacific Coasts*, Hasanuddin University Press, Bali, Indonesia, Sep. 24–26.

Drimer, N., Agnon, Y. and Stiassnie, M., 1992. A simplified analytical model for a floating breakwater in water of finite depth, *Applied Ocean Research*, 14(1), 33–41.

Elchahal, G., Younes, R. and Lafon, P., 2008. The effects of reflection coefficient of the harbour sidewall on the performance of floating breakwaters, *Ocean Engineering*, 35(11–12), 1102–1112.

Gesraha, M.R., 2006. Analysis of π shaped floating breakwater in oblique waves: I. Impervious rigid wave boards, *Applied Ocean Research*, 28(5), 327–338.

Hales, L.Z., 1981. *Floating Breakwater*: *State-of-the-Art*, *Literature Preview*, Technical Report No. TR-81–1, U.S. Army Coastal Engin-

eering Research Center, Fort Belvoir, VA.

He, F., Huang, Z.H. and Adrian, W.K.L., 2012. Hydrodynamic performance of a rectangular floating breakwater with and without pneumatic chambers: An experimental study, *Ocean Engineering*, 51, 16–27.

Ji, C.Y., Chen, X., Cui, J., Yuan, Z.M. and Incecik, A., 2015. Experimental study of a new type of floating breakwater, *Ocean Engineering*, 105, 295–303.

Koftis, T. and Prinos, P., 2005. Improved hydrodynamic efficiency of pontoon-type floating breakwaters, *Proceedings of XXXI International Conference IAHR*, IAHR, Seoul, Korea, 4047–4056.

Koraima, A.S. and Rageh, O.S., 2013. Effect of under connected plates on the hydrodynamic efficiency of the floating breakwater, *China Ocean Engineering*, 28(3), 349–362.

Koutandos, E.V., Karambas, T.V., and Koutitas, C.G., 2004. Floating breakwater response to waves action using a Boussinesq model coupled with a 2DV elliptic solver, *Journal of Waterway, Port, Coastal, and Ocean Engineering*, 130(5), 243–255.

Mani, J.S., 1991. Design of Y-frame floating breakwater, *Journal of Waterway, Port, Coastal, and Ocean Engineering*, 117(2), 105–118.

Mansard, E.P.D. and Funke, E.R., 1980. The measurement of incident and reflected spectra using a least squares method, *Proceedings of the 17th International Conference on Coastal Engineering*, Sydney, Australia, 154–172.

Moghim, M.N. and Botshekan, M., 2017. Analysis of the performance of Pontoon-type floating breakwaters, *HKIE Transactions*, 24(1), 9–16.

Murali, K. and Mani, J.S., 1997. Performance of cage floating breakwater, *Journal of Waterway, Port, Coastal, and Ocean Engineering*, 123(4), 172–179.

Peña, E., Ferreras, J. and Sanchez-Tembleque, F., 2011. Experimental study on wave transmission coefficient, mooring lines and module connector forces with different designs of floating breakwaters, *Ocean Engineering*, 38(10), 1150–1160.

Sannasiraj, S.A., Sundar, V. and Sundaravadivelu, R., 1998. Mooring forces and motion responses of pontoon-type floating breakwaters, *Ocean Engineering*, 25(1), 27–48.

Tang, H.J., Huang, C.C. and Chen, W.M., 2011. Dynamics of dual pontoon floating structure for cage aquaculture in a two-dimensional numerical wave tank, *Journal of Fluids and Structures*, 27(7), 918–936.

Weng, W.K. and Chou, C.R., 2007. Analysis of responses of floating dual pontoon structure, *China Ocean Engineering*, 21(1), 91–104.

Williams, A.N. and Abul-Azm, A.G., 1997. Dual pontoon floating breakwater, *Ocean Engineering*, 24(5), 465–478.

Yao, G.Q., Ma, Z.X. and Ding, B.C., 1993. Experimental study on rectangular floating breakwaters, *China Ocean Engineering*, 7(3), 323–332.